Bulletin of the Mineral Research and Exploration

http://bulletin.mta.gov.tr

Post-halite gypsum pseudomorphs with evidence of challenging climatic conditions and diagenetic replacement: a study from the southwest of Kağızman Basin (Eastern Anatolia, Türkiye)

Pelin GÜNGÖR YEŞİLOVA[a*]

[a] *Department of Geological Engineering, Van Yüzüncü Yıl University, 65080, Van, Türkiye*

Research Article

Keywords:
Kağızman, Gypsum, Pseudomorph, Halite, Saline-Lake.

ABSTRACT

The study area is about the evaporitic-dominated Middle Miocene sequence situated in the southwest of the Kağızman Basin in Eastern Anatolia. The aim of this study is to investigate the formation conditions and diagenetic development of pseudomorph gypsum formed after halite. Pseudomorph gypsum formations are intriguing geological features found in terrestrial deposits. These formations are replaced by primary halite crystals during the very early phases of diagenesis, giving the appearance of halite crystals but being composed of gypsum. The development of these pseudomorphs is indicative of specific paleoenvironmental conditions. The fact that these gypsum pseudomorphs are found in shallow depths of the lake and are well-preserved, smooth-surfaced, and varying in size suggests that they were the result of intense evaporation and rapid fluctuations in the water and pH level. This evaporation likely led to a decrease in the lake level and changes in the concentration of saltwater over time. The correlation coefficient relationships and element concentration values of these gypsums show that these elements are both continental in origin and subject to microbial influence. These pseudomorph gypsum and the clastic materials (transported by fluvial activity) that were interbedded gave important insights into the hot, long-drought, and low-humidity climate of the era and adapted to the Middle Miocene global warming conditions

Received Date: 22.01.2024
Accepted Date: 07.02.2024

1. Introduction

The Miocene saw significant tectonic and climatic events (Potter and Szatmari, 2009). There existed a warm period known as the Middle Miocene Climatic Optimum during the Miocene. Long-term cooling that had been occurring during the Cenozoic was broken during this time (Methner et al., 2020). High-amplitude climate variability was a defining feature of the Middle Miocene Climatic Optimum, which occurred between approximately 14.7 and 13.8 million years ago. The primary proof of this shift was found in the rise in $\delta^{18}O$ observed in the benthic foraminiferal records (e.g. Holbourn et al., 2005; Shevenell et al., 2008; Lear et al., 2010). According to paleobotanical and fossil research, temperatures were higher globally and in the East and Central Paratethys during the Langhian (Ivanov et al., 2011). Halite and gypsum are common evaporitic deposits found in the Kağızman Basin and other regions of the Central Paratethys that date back to the Middle Miocene (Rögl, 1999). The global climate and a favorable tectonic environment are responsible for the presence and distribution of the Miocene brine deposits in the Kağızman Basin (Kayseri-Özer, 2013).

Citation Info: Yeşilova, G. P. 2024. Post-halite gypsum pseudomorphs with evidence of challenging climatic conditions and diagenetic replacement: a study from the southwest of Kağızman Basin (Eastern Anatolia, Türkiye). Bulletin of the Mineral Research and Exploration 174, 111-124. https://doi.org/10.19111/bulletinofmre.1472974

**Corresponding author: Pelin GÜNGÖR YEŞİLOVA, pelingungoryesilova@yyu.edu.tr*

Furthermore, it was discovered that the Arecaceae and Lauraceae plant families were representative of the hot, subtropical climate that prevailed at the time (Kayseri-Özer, 2013). These evaporite units, which are distributed Tuzluca formation between Kağızman and Tuzluca districts (Figures 1a, b) are generally

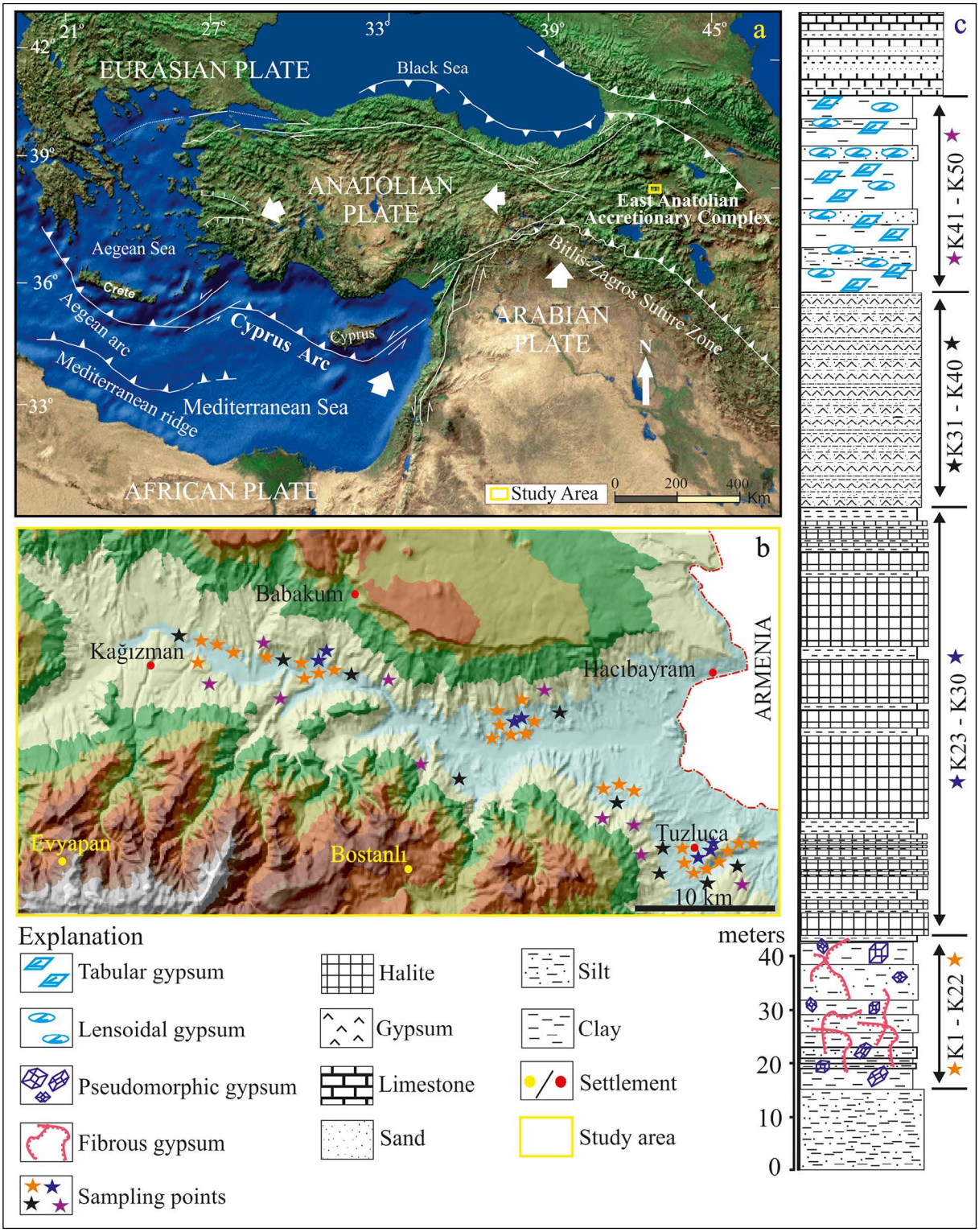

Figure 1- a) Location map of the study area, b) 1/25000 scale relief map of the study area and sampling points (from K1 K50), c) the evaporitic general succession (from bottom to top).

classified as Middle Miocene aged shallow sea-lake deposits according to their stratigraphic position (Şenalp, 1969; Jrbashyan et al., 2001; Papworth and Aghabalyan, 2002; Şen et al., 2011; Metais et al., 2015; Varol et al., 2016). Whereas Eocene sandstone, conglomerate siltstone, and limestone units form the base of these deposits, they are overlain by Pleistocene volcanic agglomerated tuff, tuffite and basalts (Havur, 1968; Yurdagül, 1971).

This study focuses on gypsum replacing halite, which developed in a shallow basin and during very early diagenetic conditions. Halite replacement with gypsum is linked to temperature variations and changes in the solubility of both minerals following chemical changes in the brine composition during the early-diagenetic dissolution–precipitation cycles (Hovorka, 1992; Schreiber and Walker, 1992). The pseudomorphic replacement of gypsum with halite is a known phenomenon and has been recorded in ancient sediments worldwide (Görgey, 1912; Schaller and Henderson, 1932; Stewart, 1949; Jones, 1965; Holdoway, 1978; Lowenstein, 1982, 1983; Warren and Kendall, 1985; Babel, 1991; Hovorka, 1992). In Türkiye and the Çankırı-Çorum Basin in Central Anatolia, it is also observed in the Late Miocene Bozkır Formation and generally is intercalated with gypsiferous mudstones and claystones (Gündoğan and Helvacı, 2001). Another example of these pseudomorphs is found in the Kağızman Basin, which constitutes our study area. Eastern Türkiye's Kağızman Basin is a compressional intermontane ramp-valley basin located east of the Karlıova Fault System, near Armenia (Şen et al., 2011). This type of pseudomorphs resulting from this diagenetic replacing are considered valuable indicators for understanding the Middle Miocene Climatic Optimum, a period of global warming. They may provide insights into the climatic conditions of the study area during that time. The gypsum pseudomorphs are more common in areas with salty units and cover an area of about 15 km^2 in the study area. This indicates that they are a significant features of the basin under investigation.

This study in Türkiye adds to the existing knowledge of such occurrences. Pseudomorphic gypsum interbedded with clastic, carbonate units within the Tuzluca Formation, located in the Kağızman Basin, have not been examined in detail before. This makes it an important research focus to understand the paleoclimatic conditions specific to this region. Therefore the goals of the study can be summarized as follows:

a) Paleoenvironmental Conditions Analysis: This aspect of the study aims to reconstruct the ancient environment in which the evaporitic sequence was deposited. It involves analyzing various sedimentological, petrographic, and geochemical data to infer factors such as climate, water depth, ecological conditions, salinity, pH levels, and the presence of organic activity during deposition.

b) Sedimentation and Diagenetic Processes: The study intends to investigate how sediments accumulated and were subsequently altered through diagenetic processes over time. Understanding these processes will provide insights into the geological history of the sequence and the transformations it underwent.

2. Methods

A total of 50 samples labeled as K1 to K50 were collected. These samples mainly consist of carbonate, silt, clay, mud-included gypsum pseudomorphs, halite, and primary gypsum (Figure 1c). Petrographic and mineralogical analyses were conducted on the collected samples. Scanning Electron Microscopy-Energy Distribution Spectroscopy (SEM-EDS) examinations were carried out at the Van Yüzüncü Yıl University Scientific Research and Application Center. Microparticles from the samples were coated with Au-Pd for 90 seconds. The samples were examined using a ZEISS Sigma 300 model SEM microscope and photographed with an SE2 detector. Elemental analyses of seven samples were conducted at ACME Analytical Laboratories in Canada. X-ray fluorescence (XRF) and inductively coupled plasma emission spectroscopy (ICP-ES) were used for elemental analysis. Concentrations in parts per million (ppm) were determined in gypsum samples using specific standards (STD DS11, STD GS 311-1, STD OREAS262, and STD SO 19) according to reference Norrish and Chappel (1977).

3. Results

3.1. Sedimentological Parameters of the Evaporitic Succession

Sedimentological parameters; the sedimentary structure was differentiated according to lithology and texture and examined by considering the lithofacies distinction. The sequence consists of a variety of sedimentary rocks, including claystone, siltstone, sandstone, limestone and evaporites (Figure 1c). Evaporites dominate and include gypsum and halite units.

In the middle and upper levels of the section, these units are intercalated and alternated with one another. Post-halite pseudomorph gypsum and selenite are the two types of gypsum that make up gypsum layers. These various gypsum species could be a sign of alterations in the mineralogical processes and depositional environment over time. Selenitic gypsums are observed in the field as transparent, white and sometimes brownish. These selenite crystals are generally observed in prismatic, tabular, lensoidal and fibrous shapes, with crystal sizes ranging from 0.5 cm to 30 cm (Figures 2a, b, c). These selenites are sometimes intercalated with clastic rocks and sometimes cemented to fill their cracks. Their fibrous filling of mud cracks indicates that they are involved in the consolidation of sediment.

Pseudomorphic gypsums, which are the subject of the study, is observed in the field, replacing halite. The cubic shape of halites is preserved. Although the cubic shape of halite is preserved, a mineralogical change is observed. These are observed intercalated with mudstones in the field (Figure 2d). Brown color is observed in places because of organic activity in these gypsum pseudomorphs buried within the compacted carbonate mud under shallow-moderate burial conditions during the early diagenesis (Figure 2d). The inner crystal surfaces of this halite, which then turns into gypsum, are hopper-shaped and concave with prominent edges (Figure 2e). Post-halite gypsum pseudomorphs size range from 2 to 20 cm in size (Figures 2f, g). Gypsum-hopper-cubes more than 10 cm in size, almost always show vertically oriented long sides and grown displacively within the soft mud (Figure 2f). Because some of these hopper-shaped gypsum-cubes became deformed during the sedimentation process due to mud compaction, the hoppers are not evident (Figure 2h). The microcrystalline primary (selenitic) gypsum formations, crystallized in dissolution cavities of a halite hopper-cube or on its surface, are macroscopically observed (Figures 2i, j). The outer surfaces of gypsum-pseudomorphs are sometimes macroscopically anhedral (Figure 2i). Partial white anhydritization areas are occasionally observed in some parts of these samples (Figure 2i). This change is a component of the diagenetic change processes, that result in the compaction of sediment from deposition and dehydration.

Halite was described as layered, banded, laminated, and sometimes primary and sometimes recrystallized. The sizes of primary halite vary between 0,5 and 20 cm. These cubes formed as the primary mineral in the sediment. Halite layers have been eroded both vertically and laterally due to the dissolution of meteoric waters. This implies a history of exposure to surface conditions and the influence of groundwater on sedimentary layers. The sequence is also included sedimentary features like folds, laminations, corrugations, and cross-beddings (Figure 1c).

3.2. Petrography and Mineralogy

In optical microscopy studies on post-halite pseudomorph gypsum samples, it is seen that primary gypsum crystals first start from the grain boundaries of the halite and then replace with halite towards the inner surface (Figures 3a, b). These gypsums are observed as small aggregates, ranging in size from a few micrometers to approximately 200 μm (Figures 3b, c). At the same time, areas, where these gypsums were partially anhydritized, were observed in some thin sections. In some thin sections, it is clearly seen that these anhydritized aggregates combine to form a nodular appearance (Figure 3c).

In some thin sections, halite was observed to show curved edges and irregular patterns forming a puzzle texture (polygonal mosaic) (Figure 3d). Within the fibrous gypsums, celestine and late diagenetic carbonate minerals (calcite and rhombohedral dolomite) were encountered in SEM-and petrographic studies (Figures 3e, f, g). In addition, traces of

Figure 2- Sedimentological properties of clay and carbonate intercalated gypsum in different lithologies in the evaporitic sequence; a) clayey-carbonate fibrous gypsum (Fg) and lensoidal gypsum (Lg), b) fine grained tabular gypsum (Tg) and prismatic gypsum, perpendicular to the bedding and organic contented, filling mud cracks, c) transparent selenite (S) with coarse grain filling mud cracks, d) smooth-surfaced with organic material content pseudomorph gypsum cube after displacively grown halite within the soft mud (brown areas: rich in organic material), e, f) pseudomorph gypsum (Psg) which hopper-shaped (Hsg) inner surface zoning and greater than 10 cm in diameter, showing long vertically oriented sides, g) pseudomorph gypsum cubes of different sizes, h) deformed gypsum pseudomorph cubes, i) selenitic gypsum (Sel) replacing halite and white anhydritization (An. areas) of these gypsum in the some areas, j) microcrystalline primary selenitic (Sel.) gypsum crystallizing in the dissolution cavities or surface of the halite cube.

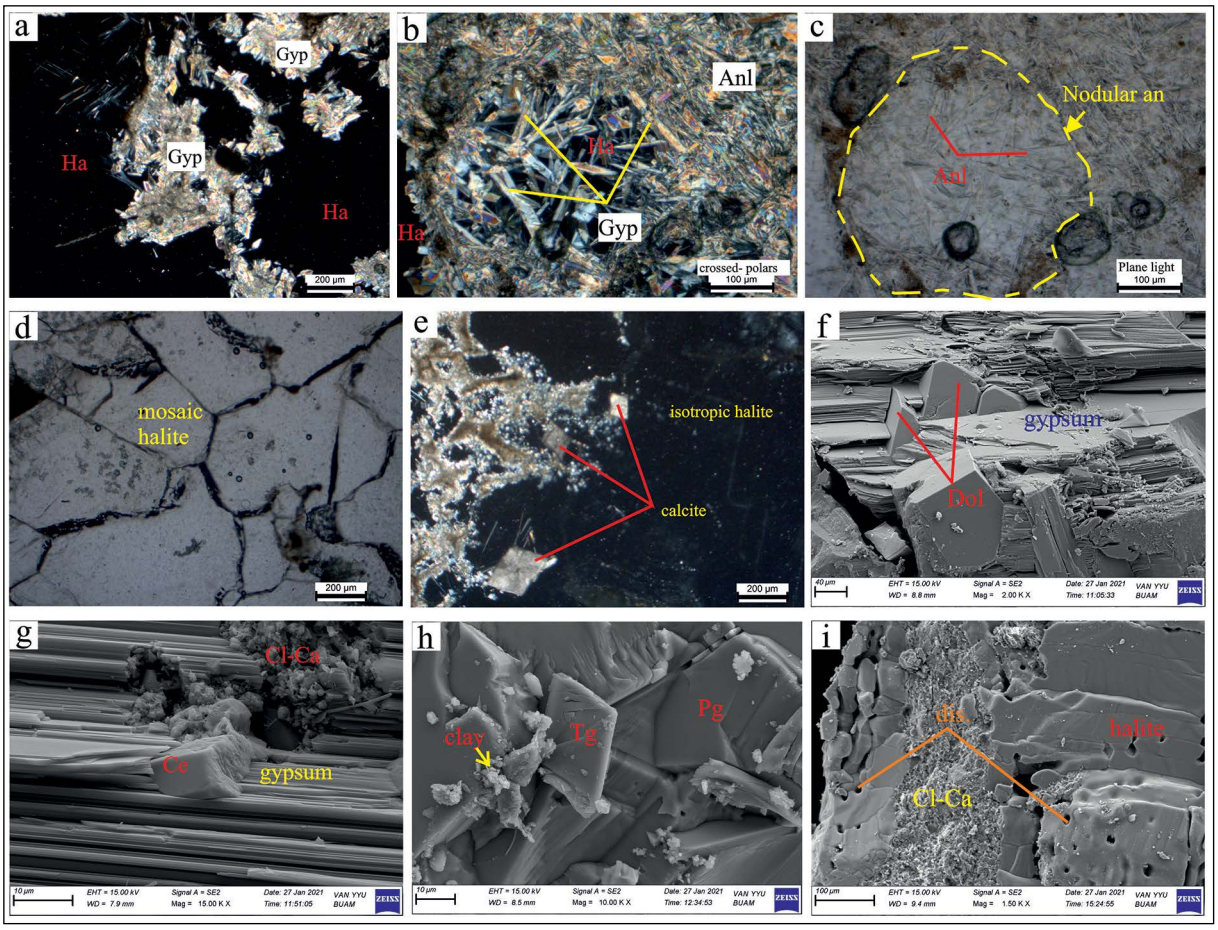

Figure 3- Optical and SEM images of carbonate-containing pseudomorph gypsum samples; a) primary gypsums observed at grain boundaries of the isotropic halite (crossed polars), b) euhedral and randomly distributed or lattice-shaped clustered gypsums (Gyp) and anhydrite laths (Anl) dispersed in or replacing halite (Ha), c) formation of anhydrite lath (Anl) aggregates and gypsum (gyp) within the anhydrite nodule (An. nodule) structure (after halite), d) polygonal mosaic-textured halite (plane light), e) secondary gypsums and euhedral calcite which developed at the margins of isotropic halites (crossed polars), f) rhombohedral dolomite (Dol) in the fibrous gypsums, g) gypsum replacing by euhedral celestine, clay-carbonate in the gypsum cracks, h) prismatic (Pg)-tabular (Tg) shaped primary gypsum with clay (smectite), i) dissolution traces (dis.) in halites with clay and carbonate (Cl-Ca) formations which filled the dissolution surfaces of these halites.

dissolution and clay and carbonate minerals filling their cracks were detected in some halite samples and tabular and prismatic gypsums (Figures 3h, i). It was found that some element contents such as Ca, Sr, Rb, Zr, Zn, Mg and Fe were at distinct peaks in the gypsum pseudomorphs (K-1, K-6 and K-10) examined in the EDS analysis (Figure 4).

3.3. Element Geochemistry

Si, Al, Fe, Na, and K major oxides in pseudomorph gypsum samples exhibit positive correlation coefficients (r^2) with each other, with values of up to $r^2 = +0.95$ (Table 1). This suggests that these elements tend to co-occur in gypsum samples. Major oxides in gypsum pseudomorph samples, specifically Si, Al, Fe, Na, and K, exhibit a negative correlation coefficient (up to $r^2 = –0.89$) with CaO. This means that, as the concentration of CaO in gypsum samples decreases, the concentrations of these major oxides tend to increase, and vice versa. Ba content in all samples is noteworthy, with Ba ratios ranging from 68 to 600 ppm (Table 1). Ba values in gypsum samples demonstrate a moderate to high positive correlation ($r^2 = +0.95$) with Rb. This indicates that Ba and Rb tend to co-occur in gypsum samples. The Sr content of pseudomorph gypsum samples was higher than other gypsum samples and increased up to approximately 3000 ppm (Table 1). Metallic elements such as Co, Ni,

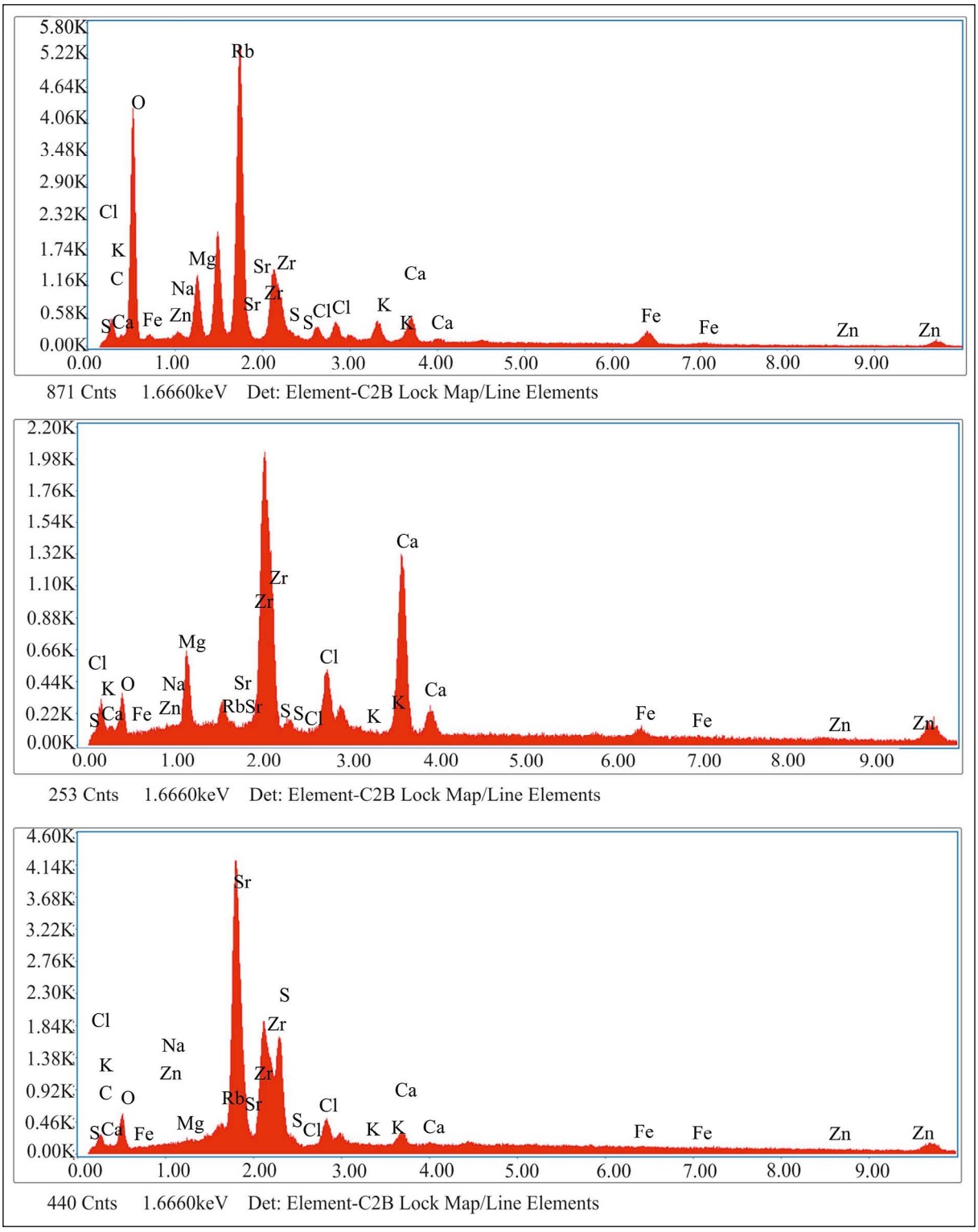

Figure 4- Element peaks in SEM-EDS analysis performed on clayey carbonate pseudomorph gypsum

Table 1- Major oxide (%) and trace element (ppm) composition of evaporites from Kağızman Basin.

Sample no	Rock type	SiO_2	Al_2O_3	Fe_2O_3	CaO	Na_2O	K_2O	Co	Ni	Cu	Zn	Zr	Mo	Ba	Sr	Rb
K-1	Pseudomorphic gypsum	9.76	2.45	1.53	25.89	3.45	0.74	16.7	33.6	72.1	85	30.1	5.9	405	1149	15.3
K-4	Pseudomorphic gypsum	1.09	1.2	0.45	32.73	0.05	0.03	3.2	18	24	5.8	13.4	2.4	600	780	30.8
K-6	Pseudomorphic gypsum	11.93	1.35	2.28	32.32	2.11	0.43	8.5	21.7	4.8	56	23.2	4.1	378	3154	14.9
K-12	Pseudomorphic gypsum	8.3	3.58	1.94	26.72	3.85	0.08	12.7	19.8	38	76	20.7	4.7	306	2405	13.7
K-15	Fibrous gypsum	3.23	1.21	0.94	31.57	0.03	0.19	2.9	15	18	6.4	12.8	1.6	500	530	24.9
K-42	Tabular gypsum	2.03	0.42	0.76	33.78	0.04	0.21	1.4	10.3	4.1	3.3	4.6	1.3	253	320	1.9
K-49	Lensoidal gypsum	2.27	1.69	0.38	32.74	0.02	0.97	1.7	13.3	4.2	7	10.2	2.6	68	440	0.5

Cu, Zn, Zr, and Mo in gypsum samples show positive correlation coefficients (r^2 = up to +0.98) with each other.

In summary, the major and trace element analysis of the gypsum and halite samples reveals various significant correlations and relationships between the elements present in these evaporite rocks. These findings can provide valuable insights into the geological and geochemical processes that have influenced the composition of these rocks.

4. Discussion

4.1. Sedimentary Environment and Diagenetic and Paleoenvironment Conditions of the Basin

4.1.1. Sedimentological and Petrographic Interpretations

Some lithofacies (massive, laminated, nodular, radial, etc.) minerals and sedimentary structures (cross-bedding, ripples, chicken-wire, etc.) in the basin provide evidence about the paleodepositional conditions (Figures 5a–g). Gypsum pseudomorphs are observed at lower levels of the geological succession, replacing old halite cubes. The variability in the texture of halite indicates that depositional conditions and diagenetic processes have changed.

With a relative increase in Ca and SO_4, the water becomes supersaturated with gypsum, and the present halite slowly begins to dissolve at 35-50°C (Hovarka, 1992; Bell and Suarez, 1993). With a further increase in temperature and salinity, it dissolves completely (Schreiber and Walker, 1992) (Figures 5h-1, 2 and 5h-3). Halite cubes (Figures 5d, 5h-1, 2), displacive growing in soft mud (host-sediment), are deformed due to sedimentation. Afterwards, dilute fluids migrate into the cubes, whose shape is preserved, and the plaster pseudomorph is formed (Figure 5h-2). Dissolution usually first concentrates at the grain boundaries of halite, then creates larger and longer voids (Figures 3a, b, 5e and 5h-3) (e.g., Shearman, 1970). Dissolution of the salt is followed by the build-up of a thin, carbonate-mud layer precipitated from brackish water, resulting from the incorporation of less saturated water immediately after a flood event (Figures 5h-2, 5h-3). These processes probably started at the surface and were completed during early diagenesis (initial stages of burial) (e.g., Casas and Lowenstein, 1989). In addition, another data showing that this early burial diagenesis took place is the presence of mosaic texture and recrystallization observed in halite (Figure 3d), (K-23-27) (Spencer and Lowenstein, 1989; Rahimpour-Bonab and Alijani, 2003; Ercan et al., 2017) (Figures 5b-c). Primary gypsum observed in some post-halite cubes loses water due to compaction in the sedimentary-early diagenetic process. It is then rehydrated first to anhydrite due to dilution of saltwaters. Then to secondary gypsum, as a result of interaction with meteoric waters. (Figures 2i, 3e). The pseudomorph gypsum cubes and selenite crystals appear various sizes (Figures 2a-b-g), indicating changes in salinity and pH conditions and mixing of different compositions of waters (marine, fresh, brackish waters) (Babel, 2004). For instance, the field-observed tabular and lenticular gypsum shapes and the brownish colors resulting from the increased organic

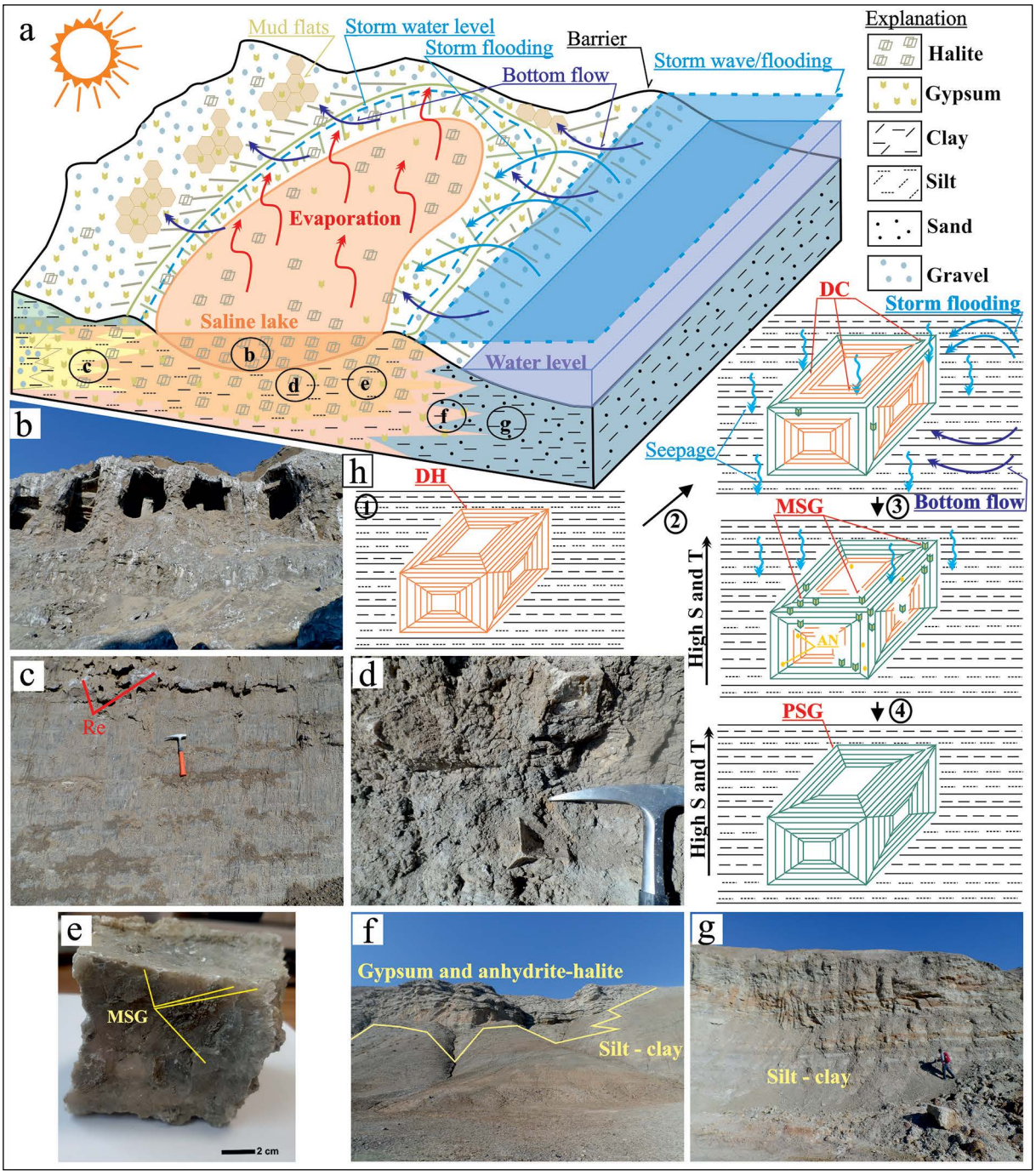

Figure 5- a) Diagram showing the depositional environments of evaporites in the study area, b) bedded halite layers (the width of the holes is about 2m), c) clayey and silty recrystallized (Re) salts, d) displacive cubic halite within the mud related to high evaporation and temperature (then replaced by gypsum), e) microcrystalline selenitic gypsum (MSG) crystals on the surface of cubic halite, f) contact boundary of gypsum and halite layers with clayey and silty units, g) silty and clayey units, h) Formation mechanism stages of pseudomorphic gypsums; 1) displacive hopper cubic halite (DH) within the soft mud, 2) dissolution cavities (DC) and minor primary gypsum that begin to replace these cavities after storm flooding and seepage, 3) microcrystalline selenitic gypsum (MSG) and minor anhydrite nodules (AN) replacing cubic halite in compacted mudstone under the high salinity (S) and temperature effects (T), 4) pseudomorphic secondary alabastrine gypsum (PSG) which formed after halite during shallow-medium burial as then rehydrated.

matter content suggest that these gypsums have a higher clay content, a slower rate of crystallization, and higher salinity, temperature, and pH levels (Cody and Cody, 1989; Calvert and Pedersen, 1996; Aref et al., 1997). In addition, the high element concentrations (Zr, Cu, Ni, Mg, Ba, Fe, Rb and Co) in the examined pseudomorphic gypsum are important, as they show that both these high salinity conditions and organic activity prevail in the basin (e.g., Averty and Paytan, 2003; Guo et al., 2019). (Figures 5g-j and Table 1). This halite-gypsum replacement occurs in hot and arid climatic conditions with low humidity and rapid, high evaporation (Logan, 1987; Leitner et al., 2013). These post-halite gypsum pseudomorphs are interpreted as products accumulating in the salty coastal lagoon and shallow inland environments (Salt Lake or Pan) (Bell and Suarez, 1993). Banded halite observed together with pseudomorphs in the evaporitic sequence support both these climatic conditions and the existence of a Salt Pan or Salt Lake environment (e.g., Rosen, 1994) that is subject to repeated floods and dilution. As a result, these pseudomorph gypsums, along with other rocks (selenite, halite, plastics, and carbonates) and sedimentary structures in the basin, evoke shallow water environments that are later irrigated by floods. Examples of these environments are salt mud flats, playa, and sabkha, which become exposed when lakes dry up. In addition, structures such as cross bedding, parallel lamination, fold corrugations and bedding in gypsum in the study area are evidence of regional tectonic, climate and strong diagenesis (Schreiber et al., 1976; Warren and Kendall, 1985; Magee, 1991).

4.1.2. Mineralogical and Geochemical Interpretations

Positive correlations between SiO_2 and other Al (r^2 = 0.52), Fe (r^2 = 0.95), Na (r^2 = 0.84) and K (r^2 = 0.18) in the major oxides and Zr/Al_2O_3 ratio (mean 10) in gypsum samples (Table 2) indicate that the paleodepositional environment became shallower due to evaporation and clastic material was carried into the basin (Pye and Krinsley, 1986; Folkoff and Meentemeyer, 1987; Haug et al., 2003; Chaudhri and Singh, 2012) (Tables 1, 2). Additionally, the negative correlations of these major oxides with CaO also support this (Table 2). The presence of these clastic materials (such as quartz, feldspar, smectite, illite, and kaolinite) was observed in SEM studies (Figures 3g-h-i). Because Zr and Si can be trapped in clastic materials such as quartz and zircon, they can easily settle in lake water under the influence of gravity (Guo et al., 2019). Therefore, the high peaks

Table 2- Correlation coefficient (r^2) relationships of major and trace elements with each other.

	SiO_2	Al_2O_3	Fe_2O_3	CaO	Na_2O	K_2O	Ni	Co	Cu	Zn	Mo	Ba	Sr	Rb	Zr
SiO_2	1,00														
Al_2O_3	0,52	1,00													
Fe_2O_3	**0,95**	0,51	1,00												
CaO	-0,60	**-0,87**	-0,53	1,00											
Na_2O	**0,84**	**0,84**	**0,82**	**-0,89**	1,00										
K_2O	0,18	0,08	-0,09	**-0,10**	0,05	1,00									
Ni	**0,72**	0,54	0,55	**-0,78**	**0,76**	0,27	1,00								
Co	**0,82**	**0,77**	**0,73**	**-0,92**	**0,96**	0,14	**0,90**	1,00							
Cu	0,41	0,64	0,29	-0,90	0,70	0,09	**0,86**	**0,84**	1,00						
Zn	0,89	0,78	**0,83**	-0,87	0,99	0,14	**0,84**	**0,98**	**0,72**	1,00					
Mo	0,83	0,77	0,70	-0,85	0,93	0,31	**0,90**	**0,96**	**0,76**	**0,96**	1,00				
Ba	0,02	-0,12	0,08	-0,09	0,00	-0,63	0,31	0,13	0,32	0,03	0,01	1,00			
Sr	0,86	0,47	0,92	-0,34	0,70	-0,13	0,41	0,57	0,08	0,70	0,62	0,08	1,00		
Rb	-0,01	0,03	0,04	-0,12	0,00	-0,56	0,29	0,11	0,30	0,01	0,04	**0,95**	0,11	1,00	
Zr	0,86	0,64	0,74	-0,79	0,85	0,22	**0,95**	**0,93**	**0,75**	**0,91**	**0,94**	0,26	0,64	0,28	1,00

observed in the SEM-EDS study (Figure 4) and the higher concentrations in the elemental geochemistry study (Table 1) prove this. This kind of clay minerals is indicative of hot-humid climates (Jackson, 1964; Foth and Truck, 1973; Singer and Navrot, 1977; Pal et al., 1989; Deepthy and Balakrishnan, 2005; Chaudhri and Singh, 2012; Corentin et al., 2019), shallow environments (such as salty, saline lakes) (Weaver, 1989) and pH fluctuations (Ingles and Anadon, 1991). Therefore, these climatic conditions are compatible with the climatic conditions prevailing during the Middle Miocene.

In the evaporation cycle, Sr can precipitate as rare strontianite ($SrCO_3$) and celestine ($SrSO_4$) (Forjanes et al., 2020). During the first stage of evaporation, brine's strontium concentration can be seen to increase. A small amount of strontium is absorbed at this stage by calcite crystallization. The Sr-concentration in the brine drops during the subsequent evaporation stage. This has to do with the crystallization of calcium sulfates, where the crystal lattice contains most of the strontium (Forjanes et al., 2020). Consequently, as shown by EDS-peaks (Figure 4) and element analyses high Sr (Table 1) in pseudomorphic gypsum is expressed by the formation of celestite replacing gypsum. At the same time, dissolved Sr^{2+} entering the lake basin usually precipitates together with carbonates in the dry period, causing a high Sr/Rb ratio (mean 222) in a humid environment (Scheffler et al., 2006; Chen et al., 2018). Therefore, the high Sr/Rb ratio in the study area (Table 1) represents a period when humid climate and continental basin conditions dominated. In addition, high Rb concentrations and peaks correspond to an increase in dolomite content in some gypsum (Scholle et al., 1992) (Figure 4 and Table 1). The high concentrations of Mo, Co, Ni, and Cu elements (Table 1) and the high positive correlations between Zn and Fe_2O_3 ($r^2 = 0.83$) mark microbiologic origins for the trace elements (Table 2) in pseudomorph-gypsums may confirm the presence of microorganisms in these gypsums and that the lake is in very salty-brackish phases (Guo et al., 2019; Patteson et al., 1986). In addition, high correlation relationships between Ni, Co, Cu, Zn and Mo elements (Table 2) indicate that the salinity in the environment is increasing (Oren, 2009). The strong positive correlation of Ba-Rb ($r^2 = 0.95$), Ni-Co ($r^2 = 0.90$), and Cu-Zn ($r^2 = 0.72$) elements refer to their continental origin (Gaillardet et al., 2004).

According to all these data, the diagenetic ranking scheme is as follows: Primary halite is formed with the lenticular and tabular gypsum during the syn-depositional stage, whereas in the early diagenetic process (shallow- burial) gypsum replaces primary halite (Figure 5h-1). At the same time, depending on flooding, halite undergoing dissolution-recrystallization processes creates a mosaic texture image. Gypsum, which later replaced the halite cube, is preserved as a pseudomorph during the early diagenetic process (shallow- moderate burial) (Figures 5e and 5h-4). Then, anhydrite, celestine, calcite and dolomite are replaced gypsum during the late diagenetic stage (exhumation). In addition, some of the clays and some siliciclastic minerals were formed during the syn-sedimentary process, whereas the other part was transported to the basin post-sedimentation by fluvials (Figures 5f-g).

5. Conclusion

The Kağızman Basin in Eastern Anatolia had a warmer, less humid climate during the Middle Miocene, according to this study. In this shallow basin, diagenetic processes, periodic flooding, drought, and rapid evaporation all had an impact. During these diagenetic processes, gypsum was replaced by minerals such as halite, anhydrite, celestite, dolomite and calcite and secondary minerals were formed. The presence of various types of selenite and smooth-surfaced, differently-sized pseudomorph gypsum suggests that the temperature, salinity and pH conditions in the basin have increased, and that a variety of waters have been mixing in the basin. Additionally, element concentrations in the basin have revealed that not only do these support the increase in salinity conditions, but there is also a microbial effect on them. The development of halite/gypsum alternation in a hypersaline environment was caused by diagenetic processes that were active during or immediately after sedimentation at surface-shallow depths. A significant amount of detrital material, consisting of feldspar grains and clay minerals, was carried to the basin by the surrounding fluvial activity during the late diagenetic phase and precipitated interbedded the evaporites.

Acknowledgements

This study was made possible with the support of The Scientific Research Project Council of Van Yüzüncü Yıl University (YYÜ, BAP, Project no: FYL-2017-5871).

References

Aref, M., Attia, O., Wali, A. 1997. Facies and depositional environment of the Holocene evaporites in the Ras Shukeir area, gulf of Suez, Egypt. Sedimentary Geology 110, 123–145.

Averty, K. B., Paytan, A. 2003. Empirical partition coefficients for Sr and Ca in marine barite, implications for reconstructing seawater Sr and Ca concentrations. Geochemistry Geophysics Geosystems 4, 1–14.

Babel, M. 1991. Dissolution of halite within the Middle Miocene (Badenian) laminated gypsum of southern Poland. Acta Geologica Polonica 41, 165–182.

Babel, M. 2004. Models for evaporite, selenite and gypsum microbialite deposition in ancient saline basins. Acta Geologica Polonica 542, 219–249.

Bell, C. M., Suarez, M. 1993. The depositional environments and tectonic development of a Mesozoic intra-arc basin, Atacama Region, Chile. Geologica Magazine 130, 395–417.

Calvert, S. E., Pedersen, T. F. 1996. Sedimentary geochemistry of manganese: Implications for the environment of formation of manganiferous black shales. Economic Geology 91, 36–47.

Casas, E., Lowenstein, T. 1989. Diagenesis of saline pan halite, comparison of petrographic features of modern, Quaternary and Permian halites. Journal of Sedimentary Petrology 59, 724–739.

Chaudhri, A. R., Singh, M. 2012. Clay minerals as climate change indicators, A case study. American Journal of Climate Change 1, 231–239.

Chen, P., Zeng, Q., Wang, Y., Zhou, T., Yu, B., Chen, J. 2018. Petrogenesis of the Dasuji porphyry Mo deposit at the northern margin of North China Craton, Constrains from geochronology, geochemistry and isotopes characteristics. Lithos 322, 87–103.

Cody, A. M., Cody, R. D. 1989. Evidence for micro-biological induction of {101} montmartre twinning of gypsum ($CaSO_4.2H_2O$). Journal of Crystal Growth 98, 721–730.

Corentin, P., Deconinck, J. F., Pellenard, P., Amédro, F., Bruneau, L., Chenot, E., Matrion, B., Huret, E., Landrein, P. 2019. Environmental and climatic controls of the clay mineralogy of Albian deposits in 2 the Paris and Vocontian basins (France). Cretaceous Research 108, 104342.

Deepthy, R., Balakrishnan, S. 2005. Climatic control on clay mineral formation, Evidence from weathering profiles developed on either side of the Western Ghats. Journal of Earth System Science 114, 545–556.

Ercan, H. Ü., Karakaya, M. Ç., Bozdağ, A., Karakaya, N., Delikan, A. 2017. Origin and evolution of halite based on stable isotopes ($\delta^{37}Cl$, $\delta^{81}Br$, $\delta^{11}B$ and $\delta^{7}Li$) and trace elements in Tuz Gölü Basin, Turkey. Applied Geochemistry 105, 17–30.

Folkoff, M. E., Meentemeyer, V. 1987. Climatic control of the geography of clay minerals genesis. Annals of the Association of American Geographers 77, 635–650.

Forjanes, P., Astilleros, J.M. and Fernández-Díaz, L. 2020. The formation of barite and celestite through the replacement of gypsum. Minerals 10, 173–189.

Foth, H. D., Truck, L. M. 1973. Fundamentals of Soil Science. Wiley, 454.

Gaillardet, J., Viers, J., Dupre, B. 2014. Trace Elements in river water. Treatise on Geochemistry 5, 25–272.

Görgey, R. 1912. Zur Kenntnis der Kalisalzlager von Wittelsheim im Ober-Elsa. Tschermaks mineralogische und petrographische Mitteilungen 31, 339–468.

Guo, P., Chiyang, L., Peng, W., Ke, W., Haili, Y., Bei, Li. 2019. Geochemical behavior of rare elements in Paleogene saline lake sediments of the Qaidam Basin, NE Tibetan Plateau. Carbonates Evaporates 34, 359–372.

Gündogan, İ., Helvacı, C. 2001. Sedimentological and petrographical aspects of Upper Miocene evaporites in the Beypazarı and Çankırı-Çorum Basins, Central Anatolia, Turkey. International Geology Review 43, 818–829.

Haug, G. H., Gunther, D., Peterson, L. C., Sigman, D. M., Highen, K. A., Aeschlimann, B. 2003. Climate and the collapse of Maya Civilization. Science 299, 1731–1735.

Havur, E. 1968. Kötek-Kağızman (Kars) çevresinin 1/25.000 ölçekli detay petrol etüdü raporu. Maden Tetkik ve Arama Genel Müdürlüğü, Rapor No: 4271, Ankara (unpublished).

Holbourn, A. E., Kuhnt, W., Schulz, M., Erlenkeuser, H. 2005. Impacts of orbital forcing and atmospheric CO_2 on Miocene ice-sheet expansion, Nature 438, 483–487.

Holdoway, K. A. 1978. Deposition of evaporites and red beds of the Nippewalla Group, Permian, Western Kansas. Kansas Geological Survey, 43.

Hovorka, S. D. 1992. Halite pseudomorphs after gypsum in bedded anhydrite – clue to gypsum-anhydrite relationships. Journal of Sedimentary Petrology 62, 1098–111.

Ingles, M., Anadon, P. 1991. Relationship of clay minerals to depositional environment in the non-marine Eocene Pontils Group, SE Ebro Basin (Spain). Journal of Sedimentary Research, 61(6), 926-939.

Ivanov, D., Utescher, T., Mosbrugger, V., Syabryaj, S., Djordjević-Milutinović, D., Molchanoff, S. 2011. Miocene vegetation and climate dynamics in Eastern and Central Paratethys (Southeastern Europe). Palaeogeography, Palaeoclimatology, Palaeoecology 304, 262–275.

Jackson, M. L. 1964. Chemical composition of soils. Bear, F. E. (Ed.). Chemistry of the soil. Reinhold Publishing Corporation. New York, 71–141.

Jones, C. L. 1965. Petrography of, evaporites from the Wellington Formation near Hutchinson, Kansas. United States Geology Survey Bulletin 1201, 1–70.

Jrbashyan, R., Chlingaryan, G., Kagramanov, Y., Karapetyan, A., Satian, M., Sayadyan, Y., Mkrtchyan, H. 2001. Geology of Meso-Cenozoic basins in Central Armenia, with comment on indications of hydrocarbons. Search and discovery article #30007.

Kayseri-Özer, M. S. 2013. Spatial distribution of climatic conditions from the Middle Eocene to Late Miocene based on palynoflora in Central, Eastern and Western Anatolia. Geodinamica Acta 26, 122–157.

Lear, C. H., Mawbey, E. M., Rosenthal, Y. 2010. Cenozoic benthic foraminiferal Mg/Ca and Li/Ca records, Toward unlocking temperatures and saturation states. Paleoceanography 25, PA4215.

Leitner, C., Neubauer, F., Marschallinger, R., Genser, J., Bernroider, M. 2013. Origin of deformed halite hopper crystals, pseudomorphic anhydrite cubes and polyhalite in Alpine evaporites (Austria, Germany). International Journal of Earth Sciences 102, 813–829.

Logan, B. W. 1987. The MacLeod evaporite basin, Western Australia: Holocene Environments, Sediments and Geologic Evolution. American Association of Petroleum Geologists Memoir, 140.

Lowenstein, T. K. 1982, Primary features in a potash evaporite deposit, the Permian Salado Formation of West Texas and New Mexico. In: Handford, C.R., Loucks, R.G., and Davies, G.R. (eds.), Depositional and diagenetic spectra of evaporites-a core workshop. Society for Sedimentary Geology, Calgary, Canada, p. 276–304.

Lowenstein, T. K. 1983. Deposition and alteration of an ancient potash evaporite, the Permian Salado Formation of New Mexico and West Texas. PhD. Thesis, The Johns Hopkins University, 411, Baltimore, Maryland.

Magee, J. W. 1991. Late Quaternary lacustrine, groundwater, aeolian and pedogenic gypsum in the Prungle Lakes, southeastern Australia. The Journal of Geology 73, 603–618.

Metais, G., Şen, S., Sözeri, K., Peigné, S., Varol, B. 2015. Late Paleogene terrestrial fauna and paleoenvironments in Eastern Anatolia, new insights from the Kağızman-Tuzluca Basin. Journal of Asian Earth Sciences 107, 96–109.

Methner, K., Campani, M., Fiebig, J., Löfer, N., Kempf, O., Mulch, A. 2020. Middle Miocene long-term continental temperature change in and out of pace with marine climate records. Scientific Reports 10, 7989.

Norrish, K., Chappel, B. W. 1977. X-ray fluorescence spectrometry. Physical Methods in Determinative Mineralogy. Zussman, J. (Ed). Clay Mineralogy. Academic Press. Cambridge, 201–272.

Oren, A. 2009. Microbial diversity and microbial abundance in saltsaturated brines: Why are the waters of hypersaline lakes red? Environment and Natural Resources Journal 15, 247–55.

Pal, D. K., Deshpande, S. B., Venugopal, K. R., Kalbande, A. R. 1989. Formation of di- and trioctahedral smectite as an evidence for paleoclimatic changes in southern and central Peninsular India. Geoderma 45, 175–184.

Papworth, T., Aghabalyan, A. 2002. Armenia's prospects 1, Armenia void of production but not without prospects. Oil and Gas Journal 100, 36–39.

Patteson, J. H, Ramsden, A. R., Dale, L. S., Fardy, J. J. 1986. Geochemistry and mineralogical residences of trace elements in oil shales from Julia Creek, Queensland, Australia. Chemical Geology 55, 1–16.

Potter, P. E., Szatmari, P. 2009. Global Miocene tectonics and the modern world. Earth Science Reviews 96, 279–295.

Pye, K., Krinsley, D. H. 1986. Diagenetic carbonate and evaporite minerals in Rotliegend aeolian sandstones of the southern North Sea: Their nature and relationship to secondary porosity. Clay Minerals 21, 443–457.

Rahimpour-Bonab, I. H., Alijani, N. 2003. Petrography, diagenesıs and depositional model for potash

deposits of north Central Iran, and use of bromine geochemistry as a prospecting tool. Carbonates and Evaporites 18, 19–28.

Rosen, M. R. 1994. The importance of groundwater in playas, A review of playa classifications and the sedimentology and hydrology of playas. Geological Society of America Special Papers 289, 1–18.

Rögl, F. 1999. Mediterranean and paratethys. Facts and hypotheses of an Oligocene to Miocene paleogeography (short review). Geologica Carpathica 50, 339–349.

Schaller, W. T., Henderson, E. P. 1932. Mineralogy of drill cores from the potash field of New Mexico and Texas. U.S. Geological Survey Bulletin 833, 1–124.

Scheffler, K., Buehmann, D., Schwark, L. 2006. Analysis of late Palaeozoic glacial to postglacial sedimentary successions in South Africa by geochemical proxies-response to climate evolution and sedimentary environment. Palaeogeography, Palaeoclimatology, Palaeoecology 240, 184–203.

Scholle, P. A., Ulmer, D. S., Melim, L. A. 1992. Late-stage calcites in the Permian Capitan Formation and its equivalents, Delaware Basin margin, west Texas and New Mexico, evidence for replacement of precursor evaporates. Sedimentology 39, 207–234.

Schreiber, B. C., Walker, D. 1992. Halite pseudomorphs after gypsum, a suggested mechanism. Journal of Sedimentary Petrology 62, 61–70.

Schreiber, B. C., Freidman, G. M., Decima, A., Schreiber, E. 1976. Depositional environments of Upper Miocene (Messinian) evaporite deposites of the Silician Basin. Sedimentology 23, 729–760.

Shearman, D. J. 1970. Recent halite rock, Baja California, Mexico. Transactions of the Institution of Mining and Metallurgy 79, 155–162.

Shevenell, A. E., Kennett, J. P., Lea, D. W. 2008. Middle Miocene ice sheet dynamics, deep-sea temperatures, and carbon cycling, A Southern Ocean perspective. Geochemistry Geophysics Geosystems 9 (2), Q02006.

Singer, A., Navrot, J. 1977. Clay formation from basic volcanic rocks in a humid Mediterranean climate. Soil Science Society of America Journal 41, 645–650.

Spencer, R. J., Lowenstein, T. K. 1989. Evaporites. Mcllreath, I. A., Morrow, D. W. (Eds.). Diagenesis II. Geoscience Canada. Reprint Series. Canada, 141–164.

Stewart, F. H. 1949. The petrology of the evaporites of the Eskdale No. 2 boring, east Yorkshire. Part I. The lower evaporite bed. Mineralogical Magazine 28, 621–675.

Şen, S., Antoine, P. O., Varol, B., Ayyıldız, T., Sözeri, K. 2011. Giant rhinoceros Paraceratherium and other vertebrates from Oligocene and Middle Miocene deposits of the Kağızman-Tuzluca Basin Eastern Turkey. Naturwissenschaften 98, 407–423.

Şenalp, M. 1969. 1/25000 scaled detailed petroleum exploration report of the Tuzluca (Kars) basin. Maden Tetkik ve Arama Genel Müdürlüğü, Rapor No: 4084, Ankara (unpublished).

Varol, B., Şen, Ş., Ayyıldız, T., Sözeri, K., Karakaş, Z., Metais, G. 2016. Sedimentology and stratigraphy of Cenozoic deposits in the Kağızman–Tuzluca Basin, northeastern Turkey. International Journal of Earth Sciences 105, 107–137.

Yurdagül, M. 1971. Kağızman doğusunun (Kars H50-c1 paftası) jeolojisi ve petrol olanakları. Maden Tetkik ve Arama Genel Müdürlüğü, Rapor No: 4828, Ankara (unpublished).

Warren, J. K., Kendall, C. G. St. C. 1985. Comparison of sequences formed in marine sabkha (subaerial) and salina (subaqueous) settings: Modem and ancient. American Association of Petroleum Geologists Bulletin 69, 1013–1023.

Weaver, C. E. 1989. Clays, Muds and Shales. Elsevier, 818.